Influence of microstructure on the hydrogen permeability of 9%Cr–1%Mo ferritic steel

N. Parvathavarthini [a], S. Saroja [b], R.K. Dayal [a,*]

[a] *Aqueous Corrosion and Surface Studies Section, Metallurgy Division, Indira Gandhi Centre for Atomic Research, Kalpakkam-603102, Tamilnadu, India*
[b] *Physical Metallurgy Section, Metallurgy Division, Indira Gandhi Centre for Atomic Research, Kalpakkam-603102, Tamilnadu, India*

Abstract

The influence of microstructure of 9%Cr–1%Mo steel on the hydrogen diffusivity, solubility and hence the permeability was investigated using electrochemical permeation technique. This steel was austenitised and cooled at various cooling rates to produce different microstructures. Tempering behaviour was also studied by heat treating for different durations at 1023 K. Characterisation of microstructures was carried out using scanning electron microscopy and analytical transmission electron microscopy. A fully martensitic product was obtained during fast cooling and a mixture of proeutectoid ferrite and martensite during slow cooling. Tempering the normalised steel resulted in the formation of fine intragranular M_2X precipitates and $M_{23}C_6$ on the boundaries. The hydrogen diffusivity and solubility showed a regular trend with the amount of strain in the lattice. Lattice defects and precipitates act as trap sites for hydrogen. Increase in lattice strain either due to increase in defect density, substructure or coherent precipitates resulted in decrease in diffusivity due to increase in trap sites. Martensite structure offered the maximum resistance to hydrogen diffusivity and tempered martensite the least resistance due to the annihilation of defects during tempering. © 1999 Published by Elsevier Science B.V. All rights reserved.

1. Introduction

9%Cr–1%Mo ferritic steel has been used for many years in the petrochemical industry for piping in the oil-fired heaters [1], gasification vessels of coal conversion plants [2], pressure vessels for coal liquefaction applications [3], and ammonia synthesis plants [4]. In recent years, this material in the normalised and tempered condition has become a favoured tubing material for fast reactor steam generators. The selection of this steel for steam generator application is based primarily on its low thermal expansion, high resistance to chloride stress corrosion cracking in water–steam systems, low decarburisation in sodium, acceptable mechanical properties at service temperatures and easy control of microstructures by simple heat treatments. Because of its

improved resistance to void swelling, irradiation creep and high temperature embrittlement, this steel is also being considered for core components applications in fast reactors.

Although this steel is always used in the normalised and tempered condition or annealed condition, microstructural changes may occur in this material either during fabrication or during service. Long term exposure at elevated temperature or excessive local heating of the tubes during faulty plant operating conditions can result in microstructural changes leading to degradation in mechanical and corrosion properties. When these steels are fusion-welded (either during fabrication or repair) sharp changes are caused in the microstructure of the weldment depending upon welding parameters. All of the above situations may result in various microstructures in the fabricated or service-exposed components quite different from the original microstructure obtained in the normalised and tempered treatment.

*Corresponding author. Fax: +91-411 440 360; e-mail: rkd@igcar.ernet.in

Hydrogen embrittlement is not a problem in this steel during services at elevated temperatures because diffusivity of atomic hydrogen in bcc/bct structures is quite high which results in drifting of hydrogen from the material. However, at ambient temperatures this steel is susceptible to hydrogen-assisted cracking during fabrication processes like welding or during storage in the corrosive coastal atmosphere. In situations when components are welded during on-site fabrication, atomic hydrogen which is absorbed in the metal during welding, can rapidly diffuse to the heat affected zone at ambient temperature and cause cold cracking even before post-weld heat treatment is performed. Cold cracking depends upon the diffusivity, solubility and hence the permeability of hydrogen in the material. Hence a thorough understanding of the hydrogen permeation behaviour under ambient conditions is necessary to avoid cold cracking.

During shutdown of plants, the components are removed and kept in ambient conditions for inspection. There is an inevitable time lag between storage, commissioning, inspection of a failure and remedial servicing before recommissioning of the plant. Hence during various stages of fabrication, storage and unscheduled shutdowns the components are exposed to the corrosive coastal atmosphere at ambient temperature. During aqueous corrosion of ferritic steel, hydrogen evolution may be one of the cathodic reactions. Corrosion-generated hydrogen can also cause hydrogen-induced stress corrosion cracking (HISCC) or degradation in ductility and toughness of the material. This involves transport of hydrogen to regions where large concentrations are built up and finally cracks are nucleated. For a crack to initiate and propagate, hydrogen has to be transported to and accumulated in an embrittlement region at or near crack tip. Therefore, the first information required to understand the mechanism of crack initiation and propagation is the rate at which hydrogen is transported in the material. The rate of entry and permeability of hydrogen determines the time required to reach a critical concentration. (Permeability is the steady state permeation rate of hydrogen through a unit thickness and unit area of the specimen at unit pressure and is equal to the product of diffusivity and solubility.) It has been reported by several authors that the rate of crack advance is controlled by the rate of supply and accumulation of hydrogen in that region [5–10]. In a type 4340 steel, it was observed that time required for failure depends on the diffusion coefficient and the activation energy for crack propagation is more or less same as that of diffusion of hydrogen [11,12].

The role of microstructure in influencing the diffusivity and solubility of hydrogen has been extensively studied. It is well known that the as-quenched, untempered martensite shows maximum susceptibility to HISCC. But the diffusivity of hydrogen in untempered martensite has been reported to be the lowest [13–16]. However, Gerberich [17] had determined apparent diffusivity (D_{app}), i.e., the hydrogen diffusivity in the presence of traps for a variety of steels and had reported one-to-one correlation between crack growth rate and D_{app} which indicates that D_{app} should be higher for martensitic structure because crack growth rate is fast. The bainitic structure had been reported to have lower permeability than pearlitic structure and the permeability of annealed and tempered microstructures had been reported to be generally high. Massive forms of carbide particles like spheroidite, globular cementite, pearlite and tempered carbides were found to offer considerably less resistance to the permeation of hydrogen [14]. Some authors had reported that, when tempering temperature is increased, permeability remained the same while the diffusivity increased [18]. This was attributed to the decrease in solubility with increase in degree of tempering. A different conclusion had been reported by another group [19]. A tempered steel with lower strength was found to have higher hydrogen solubility. Cold rolling had been found to result in lower permeability due to the presence of traps introduced during cold working. Smialowski [20] had reported that the permeability of a steel is much higher when the permeation is measured normal to the direction of rolling than when measured parallel to the rolling direction. Since controversial opinions exist among various investigators, a thorough understanding of the influence of microstructure on permeation and diffusion of hydrogen is essential in assessing susceptibility of materials to HISCC. Detailed investigations were carried out to study the influence of microstructure of 9%Cr–1%Mo steel on the hydrogen diffusivity and solubility and the results were correlated to the susceptibility to HISCC [21].

In this paper the principle of the electrochemical permeation technique is elaborated. The influence of microstructure of 9%Cr–1%Mo steel on hydrogen permeability, diffusivity and solubility has been understood. The correlation between the microstructural variations and the hydrogen permeability, diffusivity and solubility has been described in detail.

2. Principle of electrochemical permeation method

The permeation of hydrogen through metals includes adsorption, dissociation of molecular hydrogen on the metal surface, dissolution and diffusion of atomic hydrogen, recombination of the atomic hydrogen and desorption of molecular hydrogen on the metal surface. In general, a diffusion process is the rate limiting step in the

hydrogen permeation process. If the permeation surface area is large compared to the thickness, one-dimensional diffusion perpendicular to the permeation surface is considered.

According to the Fick's first law, diffusion rate of hydrogen, J (diffusion flux in unit time on unit area) is expressed as

$$J = -D\frac{dc}{dx}, \tag{1}$$

where D is the hydrogen diffusivity, dc/dx is the concentration gradient along the x-axis which is normal to the permeation surface of the membrane specimen. When steady state diffusion is attained a constant concentration gradient is established in the specimen.

At steady state,

$$J = -D\left\{\frac{C_2 - C_1}{L}\right\}, \tag{2}$$

where C_1 and C_2 are the concentrations of hydrogen at inlet and outlet surface, L is the specimen thickness. The steady state permeation rate can be accurately determined by electrochemical permeation technique which was developed by Devanathan and Stachurski in 1962 and has been widely used thereafter [22–29]. In this method, a thin specimen of the material being investigated divides the permeation cell into two compartments and serves as one surface, from which hydrogen evolves at a known rate, generally galvanostatically. The other surface (palladium coated to minimise contribution of metal dissolution to the permeation current and to maintain a uniform surface) is maintained at an anodic potential (−40 mV (Saturated Calomel Electrode)) such that the hydrogen arriving at this surface is immediately oxidised to produce a current in a potentiostatic circuit. This permeation current is recorded as a function of time. The electrochemical permeation method is advantageous over the other methods, because the experimental conditions such as temperature, potential, pH, composition of the solution etc. can be easily altered and studied. The sensitivity of this technique is about 10^{-12} g atom/cm^2/s which is comparable with that of mass spectrograph [30]. Permeation currents of about 1 μA can be readily measured which corresponds to a flux of 10^{-11} mol H/s [14]. A typical permeation transient showing the variation of permeation current with respect to time is presented in Fig. 1. Diffusion coefficients can be calculated from permeation transients by a number of methods as follows [22].

(i) If t_b is the time required for the break through in permeation current,

$$D = \frac{L^2}{15.3t_b}. \tag{3}$$
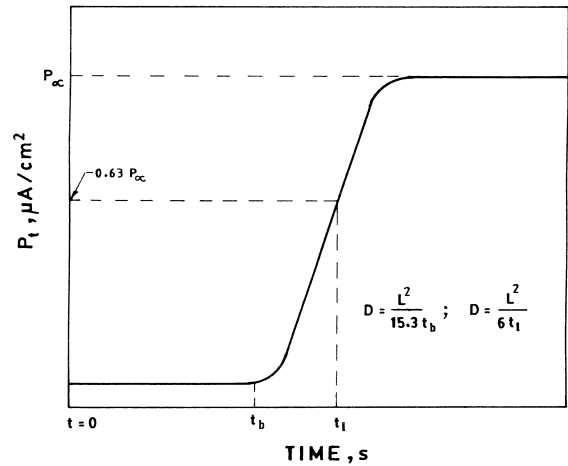
(ii) The time-lag (t_l) is related to D as follows:

Fig. 1. Schematic representation of permeation transient obtained in Devanathan–Stachurski's method.

$$D = \frac{L^2}{6t_l}; \tag{4}$$

t_l is the time needed for permeation rate to reach 63% of steady state value.

(iii) From the rise transient, a plot of $\ln((P_t - P_\infty)/P_\infty))$ against t is made which has a slope, $1/t_0$, where P_t is the permeation current at time t and P_∞ is that at steady state, and $t_0 = L^2/2D$. Then D can be calculated from the slope.

(iv) From the decay transient, a plot of $\ln(P_t/P_\infty)$ against t is made which has a slope, $1/t_0$ with the same significance as in case (iii). D can be calculated from the slope.

However, the literature relating to the hydrogen transport in steel indicates sufficient evidence to invalidate the application of Fick's law to hydrogen diffusion in steel at low temperatures due to trapping. McNabb and Foster [31] made a mathematical analysis for diffusion accompanied by trapping and untrapping. According to their assumed model, the time lag t_l is not only related to the specimen thickness (L), diffusivity (D) but is also affected by the concentration of lattice dissolved hydrogen (C), concentration of traps (N), kinetic parameters of trapping (K) and untrapping reactions (P) as follows:

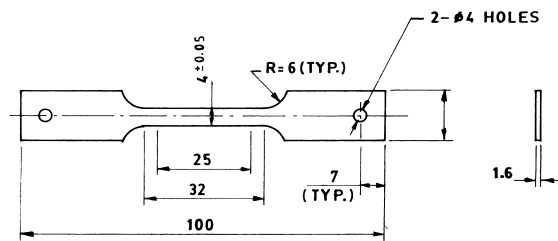$$D = \frac{L^2}{6t_l}[1 + N(K/P)]\left[1 - \frac{N[K/P]^2}{[2(1 + N(K/P))]} + \cdots\right]. \tag{5}$$

When trapping does not occur, the above equation reduces to $D = L^2/6t_l$. Thus for the more realistic cases, when trapping occurs, the D obtained from equations described earlier is apparent diffusivity (D_{app}) that includes the trapping process.

3. Experimental procedure

The material used in this investigation was nuclear grade 9%Cr–1%Mo steel forging (1000 mm diameter and 300 mm thick) and was supplied by Bruck GmbH, Germany. The chemical composition is given in Table 1. The thick section forging had been subjected to austenitising at 1223 K for 5 h followed by quenching in water. The tempering heat treatment was carried out at 1023 K for 8 h followed by air-cooling. The material in this heat-treated condition will be referred as 'as-received'. From this material, specimens of required sizes were cut for further investigations.

The specimens were sealed in a quartz tube, evacuated to 10^{-4} torr and various heat treatments were given to obtain different microstructures. The details of the heat treatments are given in Table 2. Since several heat treatment routes were adopted, each route is assigned a suitable designation which will be followed throughout the text. The microstructure of each heat treated specimen was characterised by conventional secondary electron imaging using a scanning electron microscope (Model PSEM 501).

From the heat treated steel, flat tensile specimens were machined as per the configuration given in Fig. 2. Tensile testing was carried out at room temperature using Instron Universal Testing Machine (Instron 1195) at a strain rate of 3.3×10^{-4} s^{-1}. From the tensile tests,

Table 1
Chemical composition of 9%Cr–1%Mo steel

Element	Wt%
Carbon	0.10
Silicon	0.75
Manganese	0.63
Sulphur	0.001
Phosphorus	0.02
Chromium	9.27
Molybdenum	1.07
Nickel	0.12
Nitrogen	0.019
Copper	0.10
Iron	Balance

Table 2
Details of the heat treatments

Heat treatment	Designation
1223 K/25 min – WQ	WQ
1223 K/25 min – AC	AC
1223 K/25 min – FC	FC
1223 K/25 min – AC + 1023 K/5 min – AC	AC5
1223 K/25 min – AC + 1023 K/15 min – AC	AC15
1223 K/25 min – AC + 1023 K/60 min – AC	AC60

WQ: water quenching; AC: air cooling; FC: furnace cooling.

Fig. 2. Tensile test specimen.

yield stress, ultimate tensile stress, uniform elongation, total elongation and % reduction in area were determined. The results are reported in Table 3. The values presented here are the average of three tests.

Circular specimens (diameter-25 mm and thickness-1.5 mm) were cut from various heat treated sheets for electrochemical permeation experiments. One surface of the specimen was polished up to 600 grit silicon carbide paper and was masked using an electroplating tape. The other surface of the specimen was polished upto 320 grit and was first activated by dipping in 50% HCl for 5 s. After cleaning, the specimen was immersed into a palladium plating solution (5 g $PdCl_2$ + 240 g Na_3PO_4 + 55 g $(NH_4)_3PO_4$ + 3.5 g benzoic acid in 1000 ml H_2O; pH adjusted to 9–11 by NH_4OH) at 323 K. Plating was done at a current density of 5 mA/cm^2 for 2 min. After plating, the electroplating tape from the other surface was removed and the specimen was cleaned and dried.

The analytical transmission electron microscopy studies on carbon extraction replicas of the heat treated 9%Cr–1%Mo steel was carried out using a Philips CM200 transmission electron microscope fitted with an EDAX analyser with super ultra thin window, at an operating voltage of 120 kV and probe sizes of 50–100 nm. The details of the analysis procedure is given elsewhere [32,33].

3.1. Design of permeation test assembly

A special type of specimen holder assembly and electrochemical double cell were designed and fabricated for electrochemical permeation studies.

3.1.1. Specimen holder assembly

The holder assembly consisted of a teflon housing and a threaded coupling as shown in Fig. 3(a) and (b). The specimen in the form of a circular disc was kept in the housing and the coupling was screwed on to fix up the specimen. The tightness was ensured by the teflon gaskets (Fig. 3(c)) which were kept in between the specimen and housing/coupling. The outer diameter of the coupling was machined with tapers on both ends in order to fix it up with the B-45 socket of the permeation

Table 3
Mechanical properties of 9%Cr–1%Mo ferritic steel

Heat treatment	Hardness VHN	YS MPa	UTS MPa	Elongation %
Austenitised and cooled to room temperature at different cooling rates				
WQ	447	1037	1314	2.88
AC	344	918	1246	5.79
FC	150	301	472	26.20
Normalised and tempered				
AC	344	918	1246	5.79
AC5	289	568	744	10.73
AC15	258	548	701	13.19
AC60	214	505	655	14.9

YS – yield strength.
UTS – ultimate tensile strength.
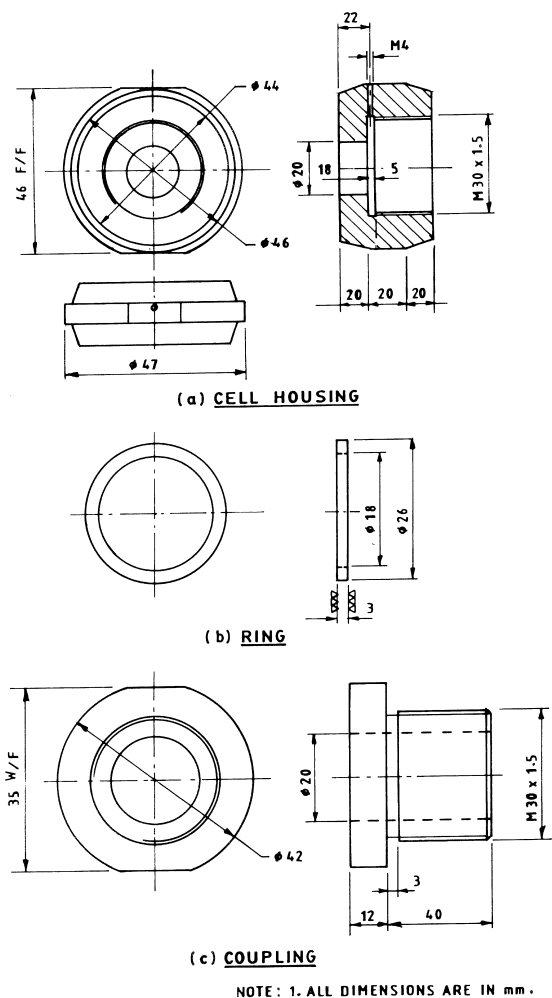
Fig. 3. Teflon holder assembly (a) cell housing; (b) ring; and (c) coupling.

cell without any leak. The housing had a threaded hole (diametrically drilled) through which electrical contact can be given to the specimen.

3.1.2. Electrochemical permeation cell

The holder assembly containing the specimen to be studied bridges two polarisation cells on either side through a B45 cone attached to the main vessel. The schematic representation of the double cell is given in Fig. 4. Out of the two cells, one was operated at anodic potential and the other side was operated at cathodic potential where hydrogen was charged by applying cathodic current galvanostatically. The cells consisted of platinised platinum auxiliary electrode assembly and luggin capillary along with saturated calomel electrode. The auxiliary electrode was kept inside a glass compartment with frittered glass disc at the bottom to avoid oxygen entry into the main vessel and to avoid increase in electrical resistance. The design of the above two assemblies ensured the following: (i) Entire system is
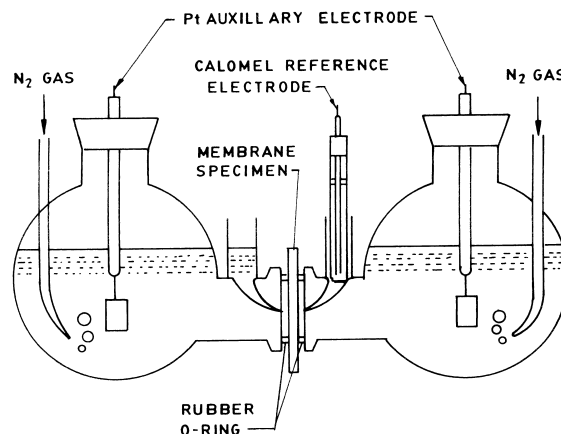

Fig. 4. Electrochemical permeation cell.

gas-tight and (ii) mix up of solutions on either side of the holder assembly is completely avoided.

The disc-shaped specimen for which hydrogen permeability is to be investigated was first assembled in the specimen holder assembly. The polarisation cells were firmly attached to the holder assembly in such a way that the palladium coated surface will be facing the anodic compartment and the as-polished surface, the cathodic compartment from where hydrogen was generated. The anodic compartment was filled with 0.1 M NaOH solution and oxygen-free dry argon gas was purged for 1 h. Then −40 mV (SCE) was applied to the specimen and the anodic current was recorded using a strip chart recorder. Within 1 h, the anodic current got stabilised. The background current was noted. Then the cathodic compartment was filled with 0.5 M H_2SO_4 solution containing 200 ppm As_2O_3. In this compartment also, argon gas was purged. Using potentiostat in galvanostatic mode, a cathodic current of 0.05 mA/cm^2 was applied. Hydrogen permeated through the specimens to the anodic side where it was instantaneously oxidised and turned into an equivalent current. Therefore, the permeation current density (P_t) at the exit side is a direct measure of the output flux of hydrogen. The variation in P_t with respect to time was monitored until steady state is reached. The rate of hydrogen permeation rises after a certain break through time (t_b) and then approaches asymptotically to the steady state permeation rate, P_∞. From the steady state permeation current density, permeability was calculated using the expression

$$P = \frac{P_\infty L}{ZF}, \tag{6}$$

where Z is the number of electrons participating in the reaction and F is Faraday's constant. The above experiments were done for all the heat treated specimens. Similar permeation experiments were carried out for as-received material at various applied cathodic current densities ranging from 0.1 to 8 mA/cm^2 to establish the relationship between permeation current and charging current.

4. Results and discussion

4.1. Characterisation of microstructures in 9%Cr–1%Mo steel

4.1.1. Transformation of austenite in 9%Cr–1%Mo steel during cooling

It is well known that 9%Cr–1%Mo steel when solutionised in the γ-phase field and cooled can transform
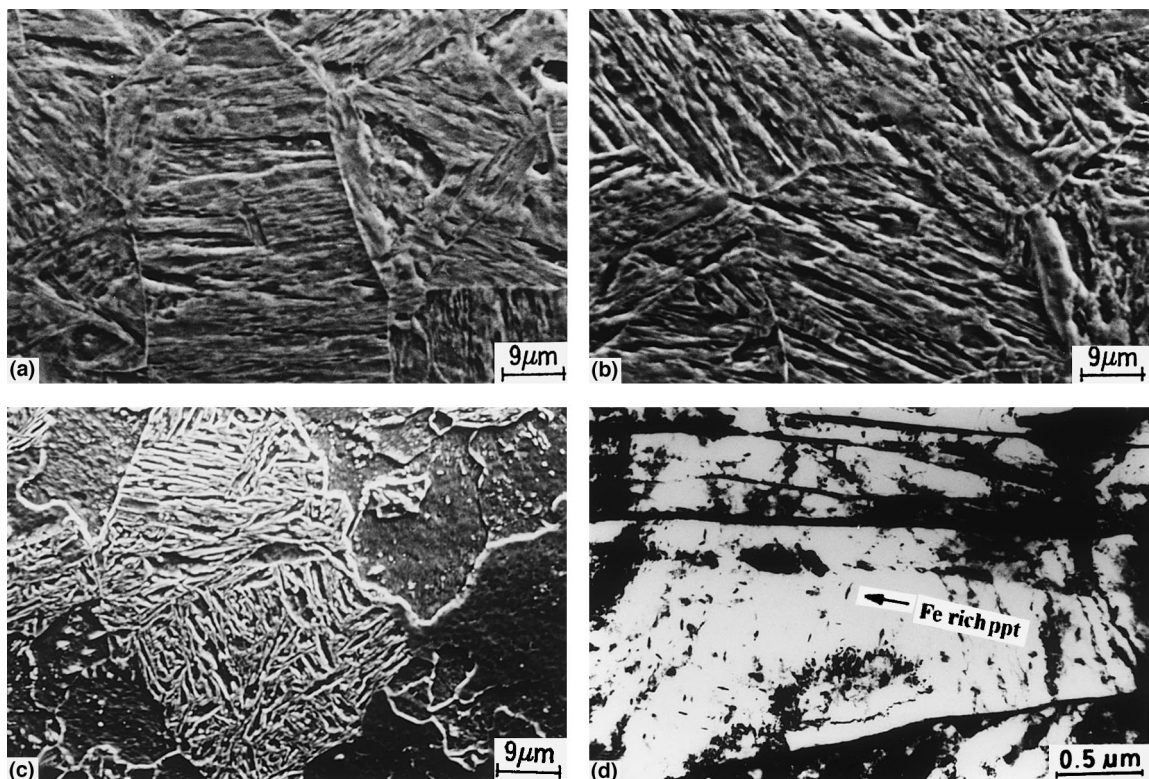

Fig. 5. Microstructures of 9%Cr–1%Mo steel (a) WQ; (b) AC; (c) FC; (d) Fe rich precipitate within ferrite grains of FC specimen [35].

to a variety of products depending on the cooling rate. The details of the microstructural characterisation of this material are reported in our earlier work [34]. Fig. 5(a)–(c) show the SEM micrographs of the steel solutionised at 1223 K and cooled by various methods ranging from water-quenching to furnace cooling. It can be seen that the microstructure consists of either martensite (for WQ and AC) or a mixture of pro-eutectoid ferrite and martensite (for FC). This is because the first two cooling rates (WQ and AC) are above the critical cooling rate for martensite formation while the third one is lower than the critical cooling rate. The martensite consists of laths or needles of ferrite aligned parallel to one another forming in bundles or packets. The observed microstructures are in complete agreement with reports [35,36] in 9%Cr–1%Mo steels for similar rates of cooling.

Table 3 shows the variation in yield strength and hardness with cooling rate. It is seen that the martensitic structure produced by the fastest cooling procedure (WQ) renders the steel with the highest strength. This can be understood in terms of the combined influence of the high defect density, fine lath substructure, high solute content (mainly carbon) characteristics of martensitic transformation all of which contribute to the high strain in the lattice to various extents. The decrease in yield strength/hardness with decrease in cooling rate (AC) is in agreement with the expected reduction in strain brought about by the softening of substructure, i.e., formation of coarser laths due to slower cooling in comparison to WQ, despite relatively high dislocation density and most of solutes in solid solution. The precipitation of a few very fine carbides during air cooling has been observed which will be described in detail in Section 4.1.2. A further decrease in yield strength/hardness in the annealed specimens (FC) is due to the formation of a soft phase namely proeutectoid ferrite along with very coarse laths as shown in Fig. 5(c). Saroja et al. [35] have established that the ferrite in this steel relieves its supersaturation with respect to carbon by precipitation of carbides within ferrite, during austenitising at 1323 K and furnace cooling (Fig. 5(d)). These precipitates have been found to be rich in iron.

4.1.2. Tempering behaviour of 9%Cr–1%Mo steel

Tempering the normalised steel at 1023 K results in a number of processes like recovery of the dislocation substructure, polygonisation of the laths and precipitation of carbides. Fig. 6 shows the transmission electron micrograph of the carbon extraction replica of this steel normalised at 1223 K and the EDAX spectra obtained from the different types of precipitates. The normalising treatment has produced a predominantly martensitic structure with some retention of pre-existing carbides in addition to precipitation of very fine carbides within the

laths (Fig. 6(a)). Fig. 6(b) shows the EDAX spectra from one of the pre-existing carbides, confirming that they are essentially Cr rich with sufficient solubility for Fe and Mo. These carbides have earlier been established by diffraction analysis as $M_{23}C_6$ type [32]. Fig. 6(c) shows the EDAX spectrum obtained from one of the fine interlath carbides. It can be seen that these carbides are rich in iron though they contain sufficient amounts of Cr and Mo. It is reported that these carbides are also of $M_{23}C_6$ type only [33].

The presence of pre-existing carbides during air-cooling is as expected due to the low austenitising temperature adopted in the present study. The presence of Fe rich carbides which are freshly nucleated can be explained based on the short time of stay in the carbide forming temperature regime due to fast cooling. Table 4 lists the details of the carbides that form during normalising and tempering of this steel.

Fig. 7(a) shows the micrograph of the carbon extraction replica of the steel tempered at 1023 K for 5 min. It can be seen that tempering leads to rejection of solute carbon, leading to precipitation of very fine carbides at dislocations and on the lath and grain boundaries. After 5 min of tempering it is seen that the lath boundaries are decorated with fine carbides with very few carbides forming within the laths which is shown in Fig. 7(a). An EDAX spectrum from a typical carbide shows that they are Cr rich with Fe and Mo (Fig. 7(b)), typical of $M_{23}C_6$ type of carbides. Further tempering up to 15 min leads to fresh nucleation of many fine intragranular carbides and precipitation of carbides along prior austenite and lath boundaries (Fig. 7(c) and (d)).

Tempering for 60 min (Fig. 8(a)) resulted in considerable reversion of martensite, formation of medium to coarse carbides on austenite and lath boundaries and also a few coarse intralath precipitates. A microdiffraction pattern from one of the intralath precipitates given as an inset in Fig. 8(a) confirms that they are of M_2X type. The diffraction pattern from a coarse interlath precipitate also shown as an inset in Fig. 8(a) confirms they are of $M_{23}C_6$ type. The EDAX spectra from the two types of precipitates, namely intralath and interlath precipitate are shown in Fig. 8(b) and (c). It can be seen that the M_2X precipitates have a very high Cr content while the interlath $M_{23}C_6$ type of carbides, though are Cr rich accommodate appreciable amounts of Fe and Mo (Table 4). The high Cr content of M_2X is a finger print of this type of carbides and serves as a guide line to distinguish between the two types of carbides. The above results are in complete agreement with earlier reports in 9%Cr–1%Mo steels [33,35].

The microstructure of 9%Cr–1%Mo can be summarised as follows.

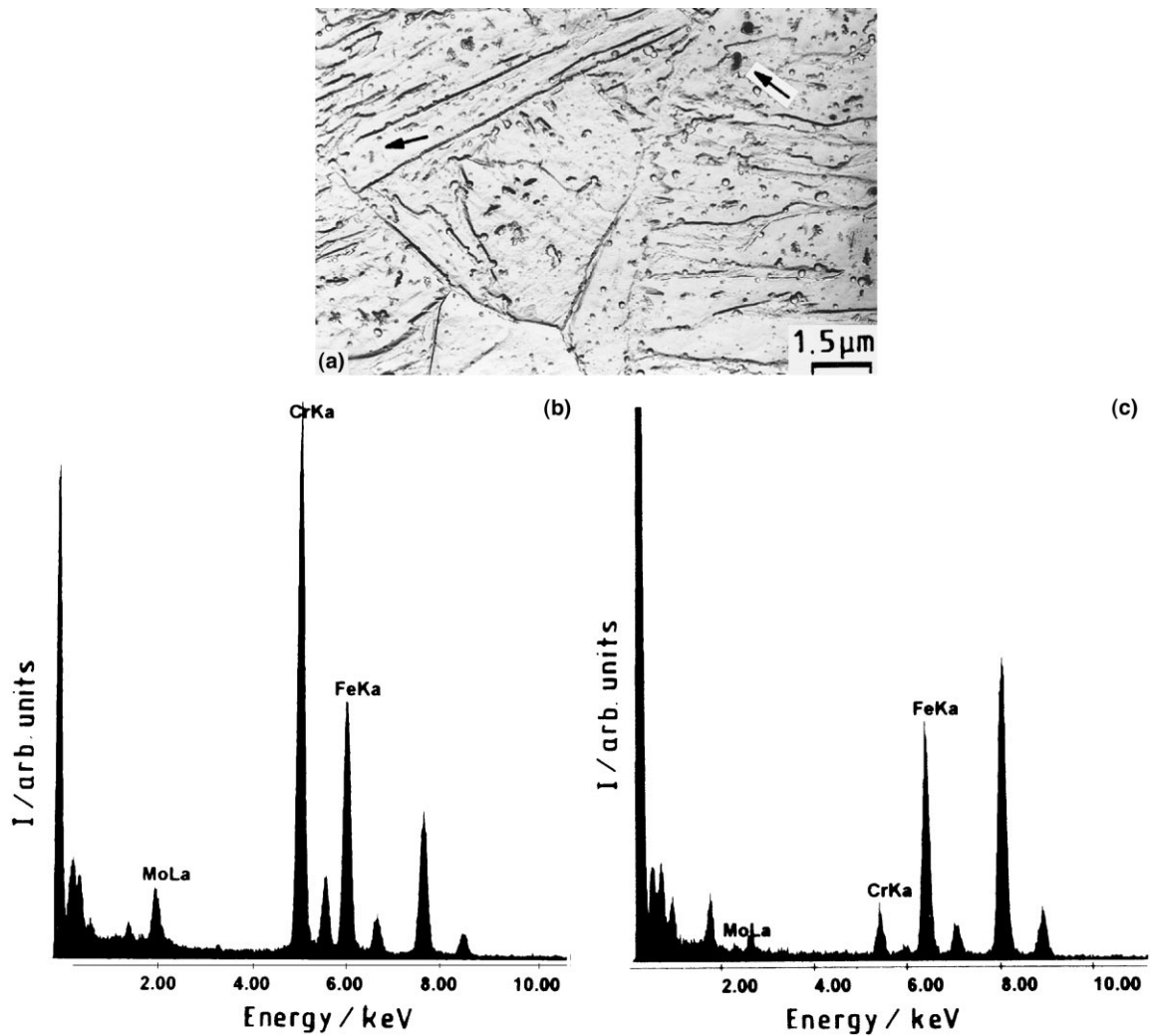1. A fully martensitic product is obtained during fast cooling and a mixture of proeutectoid ferrite and

Fig. 6. (a) TEM micrograph of the carbon extraction replica of 9%Cr–1%Mo steel normalised at 1223 K showing the presence of pre-existing carbides and fine intralath carbides, (b) EDAX spectrum from a pre-existing carbide shown in (a), (c) EDAX spectrum from one of the fine intralath carbides shown in (a).

Table 4
Microchemical data for the carbides in 9%Cr–1%Mo ferritic steel

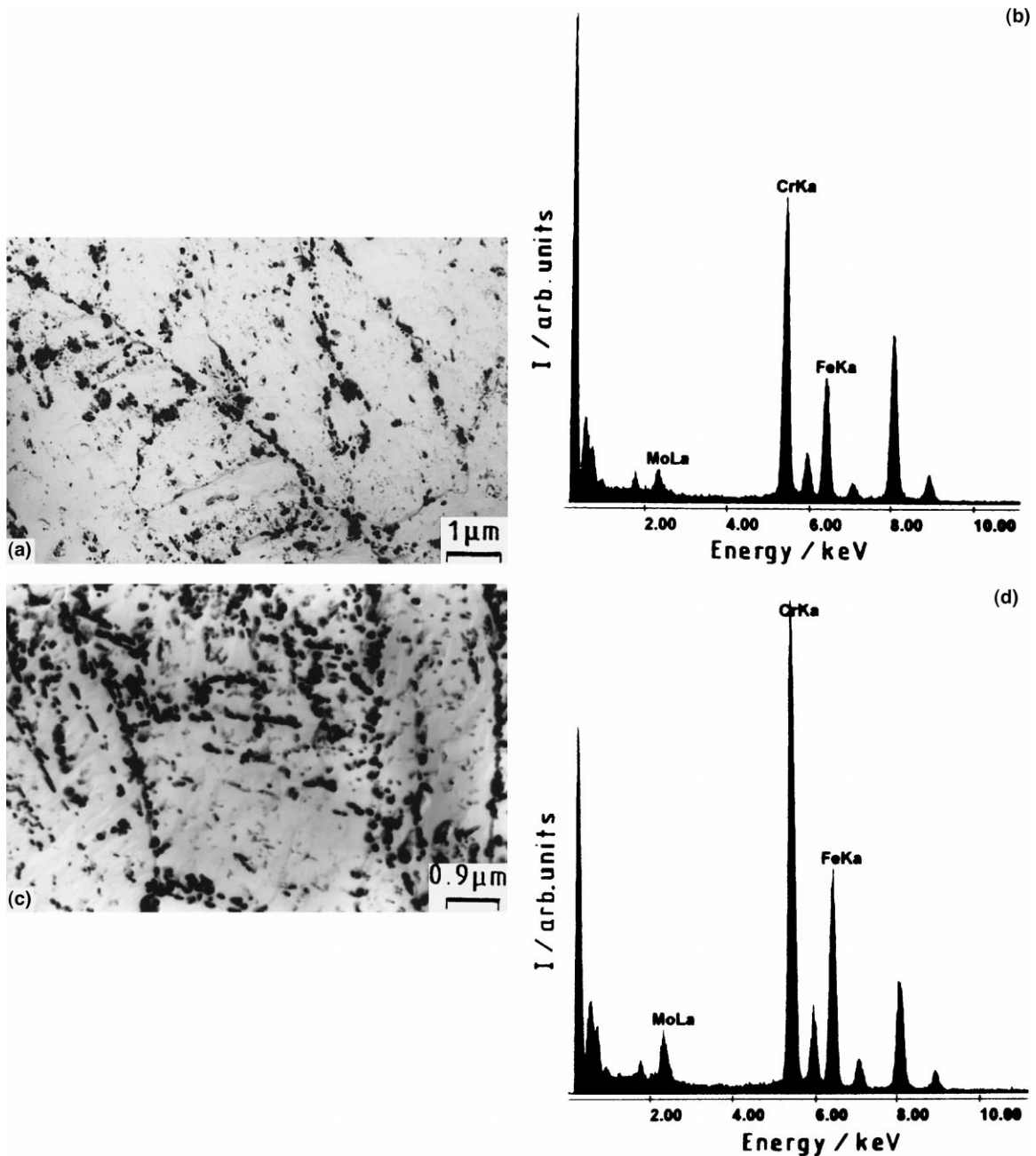| Heat treatment	Type of carbides	Description	Microchemistry at.% of elements in metal lattice		
			Fe	Cr	Mo
AC	$M_{23}C_6$	Pre-existing	30.4	58.8	10.9
	$M_{23}C_6$	Intralath	80.4	13.9	5.9
AC5	$M_{23}C_6$	Intralath	26.7	64.1	9.2
AC15	$M_{23}C_6$	Intralath	27.6	61.4	13.4
AC60	M_2X	Intralath	4.3	89.2	6.6
	$M_{23}C_6$	Lath boundary	22.9	62.5	14.6

Fig. 7. (a) TEM micrograph of the carbon extraction replica of 9%Cr–1%Mo steel normalised at 1223 K and tempered at 1023 K for 5 min showing the lath boundary and a few intralath carbides, (b) EDAX spectrum from a representative carbide shown in (a), (c) TEM micrograph of carbon replica of 9%Cr–1%Mo steel normalised at 1223 K and tempered at 1023 K for 15 min showing the lath boundary carbides and a large number of intralath carbides, (d) a typical EDAX spectrum from one of the carbides shown in (c).

martensite during slow cooling with retention of some pre-existing carbides.

2. Tempering the normalised steel results in formation of fine intragranular and boundary carbides all of $M_{23}C_6$ type.

3. Precipitation of Cr rich M_2X within laths is seen after tempering for 60 min.

4. The combined effect of dislocation density, substructure, precipitate type and morphology is reflected in the yield strength and hardness values.
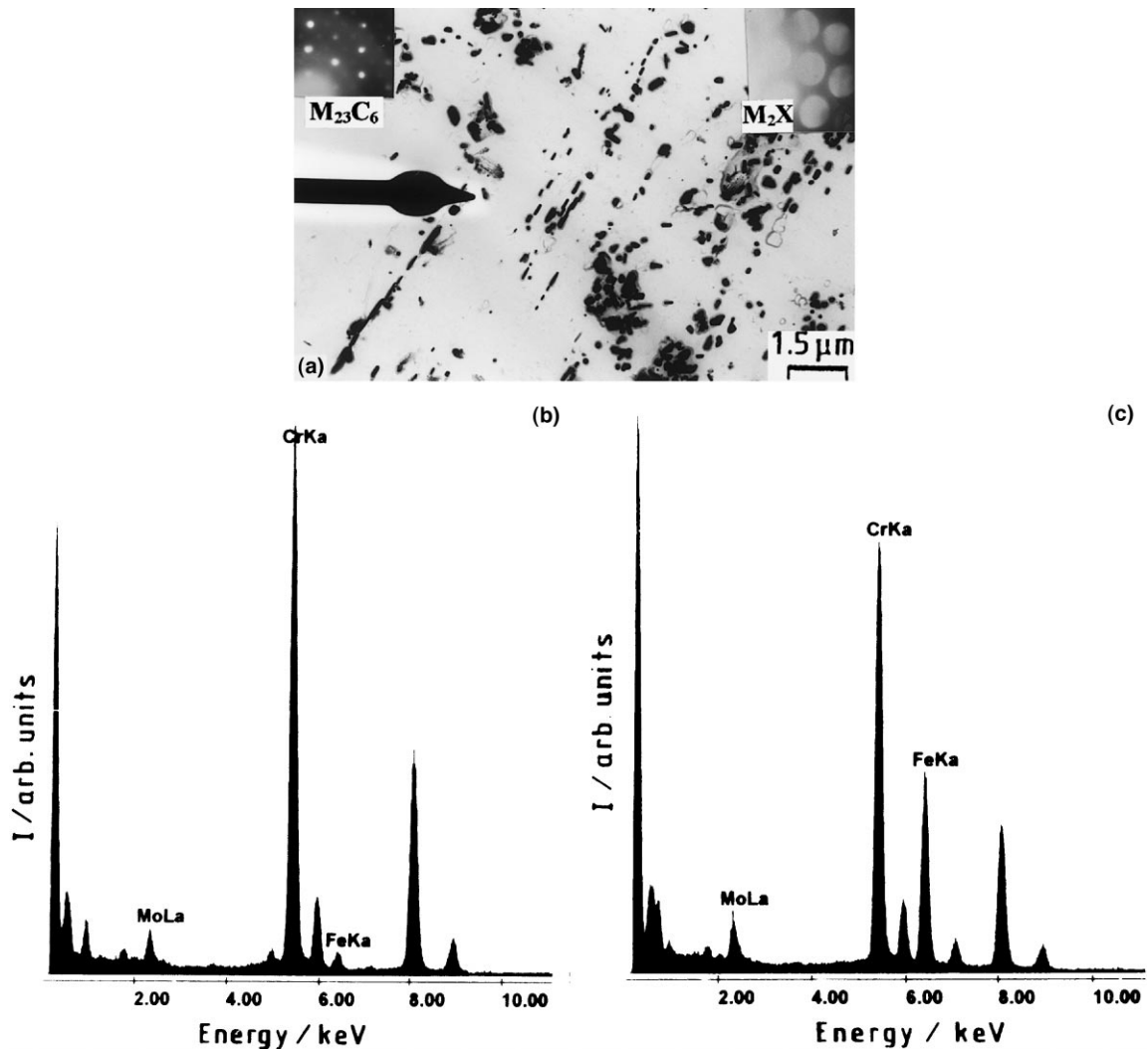
Fig. 8. (a) TEM micrograph of the carbon replica of 9%Cr–1%Mo steel normalised at 1223 K and tempered at 1023 K for 60 min showing coarse intralath and interlath precipitates. The insets show the electron diffraction patterns from an interlath carbide confirming that it is $M_{23}C_6$ type along $\langle \bar{1}\,\bar{1}\,1 \rangle$ zone axis and an intralath carbide (arrow marked in figure) confirming that it is M_2X along $\langle 0\,1\,\bar{1}\,0 \rangle$ zone axis and (b,c) EDAX spectra from M_2X (arrow marked) and $M_{23}C_6$. The high Cr content in M_2X serves as a finger print to distinguish between two types of precipitates.

4.2. Electrochemical permeation studies

For the as-received material, the permeation current density determined in 0.5 M H_2SO_4 containing 200 ppm As_2O_3 at various applied current densities ranging from 0.1 to 8 mA/cm^2 is shown in Fig. 9. The permeation current density followed a square root dependence with charging current density.

The permeation transients obtained for all the heat treated specimens are collectively presented in Fig. 10(a) and (b). From the breakthrough time, D_{app} was calculated using Eq. (3). Permeability (p) was calculated from the steady state permeation current density using Eq. (6). From D_{app} and p, solubility (S) was calculated, since $p = d_{app}s$. The results are consolidated in Table 5.

The true diffusivity of hydrogen in α-iron is of the order of 10^{-5} cm^2/s and diffusivity of low alloy ferritic steel is about the same as that of α-iron [37]. Since for this steel, diffusivity is three orders of magnitude lower, the presence of traps can be inferred. The D_{app} represents the diffusivity of lattice dissolved and reversibly trapped hydrogen. The solubility corresponds to the hydrogen in lattice and reversible traps. The steady state permeability gives the overall effective permeability.

The variation in diffusivity and solubility for different microstructures show a systematic trend as can be seen
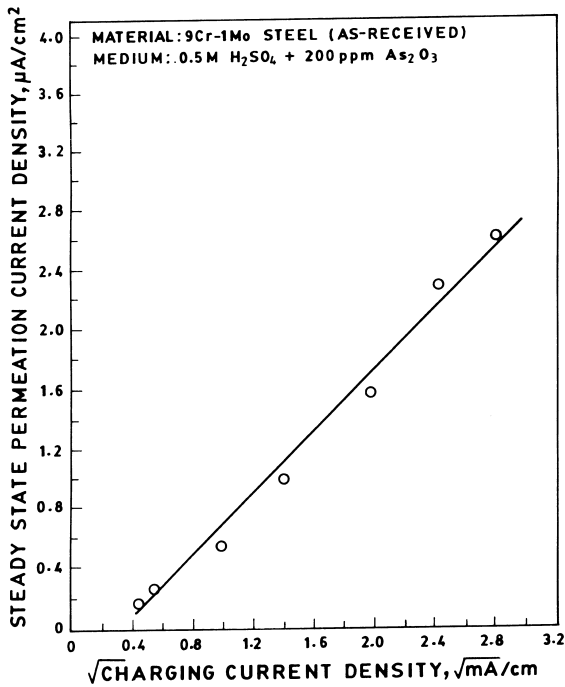
Fig. 9. Variation of steady state permiation current density with charging current density.

from Table 5. The martensitic structure obtained by water quenching has the highest solubility and hence lowest diffusivity. This can be attributed to the complex microstructure of martensite which has a high degree of strain due to the carbon atoms retained in the α-iron lattice in addition to the high dislocation density introduced during fast quenching. Autoradiographic studies using tritium tracers [38,39] have shown that hydrogen gets trapped at dislocations, point defects, subgrain boundaries, voids, lath boundaries, precipitate/matrix interfaces etc or at any other feature that can introduce strain in the lattice. Additionally prior austenite grain boundaries and triple points also act as trap sites for hydrogen.

The decrease in solubility and the consequential increase in diffusivity for AC and FC specimens is as expected. The reduction in strain due to decrease in defect density and the coarse substructure as a consequence of slower cooling rates manifests itself as decrease in the number of trapping sites for hydrogen. This has brought about the observed decrease in solubility and increase in the apparent diffusivity. The presence of the softer pro-eutectoid ferrite phase, apart from the large reduction in defect density is responsible for the high values of D_{app} in FC specimens. This is reflected in the overall increase in the permeability compared to that in AC specimen.

It is well known that fine carbides also act as trapping sites for hydrogen, which would lead to an increase in
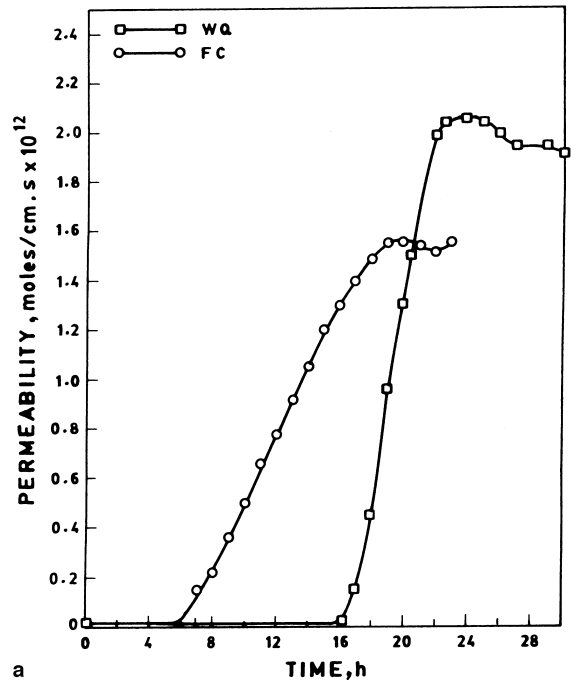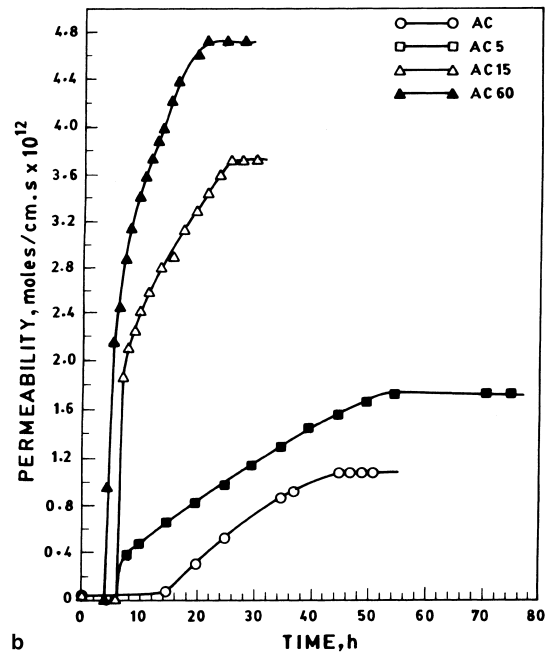
Fig. 10. (a) Permeation curves of WQ and FC specimens of 9%Cr–1%Mo steel in 0.5 M H_2SO_4 containing 200 ppm As_2O_3 ($i_c = 0.05$ mA/cm^2). (b) Permeation curves of normalised and tempered specimens of 9%Cr–1%Mo steel in 0.5 M H_2SO_4 containing 200 ppm As_2O_3 ($i_c = 0.05$ mA/cm^2).

the solubility. However in the present study no such increase in solubility was observed in the AC and FC specimens though the presence of very fine intralath

Table 5
Hydrogen permeability (p), diffusivity (D), solubility (S) of 9%Cr–1%Mo ferritic steel in 0.5 M H_2SO_4 containing As_2O_3 ($i_c = 0.05$ mA/cm^2)

Sample	$p \times 10^{12}$ mol/cm s	$D \times 10^8$ cm^2/s	$S \times 10^4$ mol/cm^3
Austenitised and cooled at different rates			
WQ	2.01	1.13	1.78
AC	1.08	1.30	0.83
FC	1.56	3.03	0.52
Normalised and tempered			
AC	1.08	1.30	0.83
AC5	1.74	2.91	0.60
AC15	3.72	2.91	1.28
AC60	4.72	4.54	1.04

carbides has been observed. This could be explained in terms of the very weak trapping of the carbides due to their low number density and fine sizes. The effect of the reduction in defect density and substructure changes far outweigh the possible increase in solubility due to precipitates resulting in the presently observed trend of a continuous decrease in solubility.

It can be seen from the last four rows in Table 5 that diffusivity increases during the initial stages of tempering which is in agreement with the expected annihilation of lattice defects during tempering. The initial stages of tempering brings about the nucleation of fine carbides along boundaries and within the laths which are very few in number. Hence they do not introduce an observable residual microstrain in the lattice. Hence these precipitates act as weak trap sites for hydrogen. The reduction in defect density and solute content dominate over these precipitation effects. Hence decrease in solubility and increase in diffusivity was observed. The permeability of hydrogen increases at the initial stages of tempering.

Tempering up to 15 min results in the increase in the number density and size of the precipitates. The strain introduced in the matrix due to the large number of fine intralath precipitates results in the carbide/matrix interfaces acting as strong trapping sites. This results in the observed increase in solubility.

Further tempering up to 60 min results in coarsening/ spheroidisation of precipitates thereby losing their coherency with the matrix as also reflected in the yield strength and hardness. $M_{23}C_6$ precipitates which form on the lath or grain boundaries are coarse and few in number and so are the M_2X precipitates. So the resultant strain in the lattice reduces bringing about a large reduction in the number of trapping sites. This is clearly reflected in the decrease in solubility and increase in D_{app} and permeability. The role of M_2X though not very clear, it can be inferred that the precipitates have very limited influence on the solubility of hydrogen and it is

the lattice defects that are the dominant features which govern the diffusivity and solubility.

In essence, these investigations reveal:
1. Microstructural features which contribute to lattice strain such as defect density, substructure and precipitates exert a strong influence on the hydrogen permeability in 9%Cr–1%Mo steels.
2. Lattice defects and precipitates act as strong traps for hydrogen. Increase in lattice strain either due to increase in defect density or coherent precipitates results in decrease in diffusivity and hence increase in solubility.

5. Summary

The influence of microstructure on the hydrogen permeability, diffusivity and solubility of 9%Cr–1%Mo steel has been studied. The hydrogen permeation studies were carried out using Devanathan's method. The results suggest that lattice defects act as most effective traps for hydrogen. The martensitic structure obtained both in water-quenched and normalised 9%Cr–1%Mo steel offered the maximum resistance to hydrogen permeability. The permeation experiments indicated that hydrogen permeability and D_{app} show an ascending trend with increase in degree of tempering due to the annihilation of lattice imperfections (which are trap sites) during tempering suggesting that precipitates have a limited influence on hydrogen permeability.

Acknowledgements

References

[1] F. Pollard, in: Ashok K. Khare (Ed.), Proceedings of ASM International Conference on Production, Fabrication, Properties and Application of Ferritic Steels for High Temperature Applications, Warren, Pennsylvania, 6–8 October 1981, p. 153.

[2] S.K. Verma, in: Ashok K. Khare (Ed.), Proceedings of ASM International Conference on Production, Fabrication, Properties and Application of Ferritic Steels for High Temperature Applications, Warren, Pennsylvania, 6–8 October 1981, p. 236.

[3] D.A. Canonico, in: Ashok K. Khare (Ed.), Proceedings of ASM International Conference on Production, Fabrication, Properties and Application of Ferritic Steels for High

Temperature Applications, Warren, Pennsylvania, 6–8 October 1981, p. 31.

[4] E.G. Nisbett, in: Ashok K. Khare (Ed.), Proceedings of ASM International Conference on Production, Fabrication, Properties and Application of Ferritic Steels for High Temperature Applications, Warren, Pennsylvania, 6–8 October 1981, p. 21.

[5] R.A. Oriani, P.H. Josephic, Acta Metall. 22 (1974) 1065.

[6] R.A. Oriani, P.H. Josephic, Acta Metall. 25 (1977) 979.

[7] W.W. Gerberich, Y.T. Chen, St.C. John, Metall. Trans. 6A (1975) 1485.

[8] W.W. Gerberich, Y.T. Chen, St.C. John, Metall. Trans. 6A (1975) 271.

[9] H.P. Van Leeuwen, Corrosion 31 (1975) 154.

[10] H.P. Van Leeuwen, Corrosion 29 (1973) 197.

[11] T.K.G. Namboodhiri, Hydrogen embrittlement, in: Proceedings of National Workshop on Stress Corrosion Cracking, RRC, Kalpakkam, 6–8 August 1980.

[12] T.K.G. Namboodhiri, Trans. SAEST 3 (1978) 177.

[13] A.W. Thompson, I.M. Bernstein, The role of metallurgical variables in hydrogen assisted environment fracture, in: M.G. Fontanna, R.W. Stahle (Eds.), Advances in Corrosion Science and Technology, vol. 7, Plenum, New York, 1980.

[14] R.D. McCright, in: R.W. Stahle, J. Hochman, R.D. McCright, J.E. Slater (Eds.), Proceedings of International Conference on Stress Corrosion Cracking and Hydrogen Embrittlement of Iron Base Alloys, 42, Unieux-Firminy, France, 1973, p. 306.

[15] T.P. Radhakrishnan, L.L. Shreir, Electrochim. Acta 12 (1967) 889.

[16] Y. Sakamoto, T. Mantani, Trans. Jpn. Inst. Met. 17 (1976) 743.

[17] W.W. Gerberich, Hydrogen in metals, in: I.M. Bernstein, A.W. Thompson (Eds.), International Conference, September 1973, Champion, PA, USA, ASM, 1974, p. 115.

[18] C.D. Kim, A.W. Loginow, Corrosion 24 (1968) 313.

[19] K. Bolton, L.L. Shreir, Corros. Sci. 3 (1963) 17.

[20] M. Smialowski, in: Proceedings of Conference on Stress Corrosion Cracking and Hydrogen Embrittlement of Iron Base Alloys, NACE, 1977, p. 405.

[21] N. Parvathavarthini, PhD thesis, Madras University, Madras, 1997.

[22] M.A.V. Devanathan, Z. Stachurski, Proc. Roy. Soc. London 270A (1962) 90.

[23] P.T. Wilson, Z. Szklarska-Smialowska, M. Smialowska, in: I.M. Bernstein, A.W. Thompson (Eds.), Hydrogen Embrittlement in Metals, AIME, 1980, p. 961.

[24] J.O.M. Bockris, J. McBreen, L. Nanis, J. Electrochem. Soc. 112 (1965) 1025.

[25] S.I. Pyun, R.A. Oriani, Corros. Sci. 29 (1989) 485.

[26] C. Kato, H.J. Grabke, B. Egert, G. Panzner, Corros. Sci. 24 (1984) 591.

[27] J.C. Turn, Jr., B.E. Wilde, C.A. Troiamos, Corrosion 39 (1983) 364.

[28] J. McBreen, M.A. Genshaw, in: Proceedings of the International Symposium on Stress Corrosion Cracking, NACE, Houston, TX, 1967, p. 51.

[29] B.E. Wilde, C.D. Kim, J.C. Turn Jr., Corrosion 38 (1982) 515.

[30] W. Beck, J.O.M. Bockris, M.A. Genshaw, P.K. Subramaniam, Metall. Trans. 2 (1971) 883.

[31] A. McNabb, P.K. Foster, Trans. AIME 227 (1963) 618.

[32] S. Saroja, M. Vijayalakshmi, V.S. Raghunathan, Mater. Trans., Jpn. Inst. Met. 34 (1993) 901.

[33] M. Vijayalakshmi, S. Saroja, V. Thomas Paul, R. Mythili, V.S. Raghunathan, submitted.

[34] N. Parvathavarthini, R.K. Dayal, J.B. Gnanamoorthy, Corrosion 52 (1996) 540.

[35] S. Saroja, M. Vijayalakshmi, V.S. Raghunathan, J. Mater. Sci. 27 (1992) 2389.

[36] S. Saroja, M. Vijayalakshmi, V.S. Raghunathan, Mat. Sci. Eng. A 154 (1992) 59.

[37] K. Kiuchi, R. McLellan, Acta Metall. 31 (1983) 961.

[38] T. Asaoka, in: Proceedings of Second JIM International Symposium on Hydrogen in Metals, Minakami, Japan, 1979, p. 161.

[39] T. Asaoka, in: Nejat, Vezivoglu (Eds.), Proceedings of Miami International Symposium on Metal Hydrogen system, 13–15 April 1981, Miami Beach, USA, Pergamon Press, Oxford, 1982.